MARTIN MARIETTA ENERGY SYSTEMS LIBRARIES

3 4456 0331054 8

ORNL/TM-11701

ornl

OAK RIDGE NATIONAL LABORATORY

MARTIN MARIETTA

Mercier Stability and Transport Properties of the URAGAN-2M and ATF Torsatrons

N. Dominguez
B. A. Carreras
V. E. Lynch
J. S. Tolliver
V. E. Bykov
D. L. Grekov
A. A. Shishkin

OAK RIDGE NATIONAL LABORATORY
CENTRAL RESEARCH LIBRARY
CIRCULATION SECTION
4500N ROOM 175
LIBRARY LOAN COPY
DO NOT TRANSFER TO ANOTHER PERSON
If you wish someone else to see this report, send in name with report and the library will arrange a loan.

MANAGED BY
MARTIN MARIETTA ENERGY SYSTEMS, INC.
FOR THE UNITED STATES
DEPARTMENT OF ENERGY

This report has been reproduced directly from the best available copy.

Available to DOE and DOE contractors from the Office of Scientific and Technical Information, P.O. Box 62, Oak Ridge, TN 37831; prices available from (615) 576-8401, FTS 626-8401.

Available to the public from the National Technical Information Service, U.S. Department of Commerce, 5285 Port Royal Rd., Springfield, VA 22161.

This report was prepared as an account of work sponsored by an agency of the United States Government. Neither the United States Government nor any agency thereof, nor any of their employees, makes any warranty, express or implied, or assumes any legal liability or responsibility for the accuracy, completeness, or usefulness of any information, apparatus, product, or process disclosed, or represents that its use would not infringe privately owned rights. Reference herein to any specific commercial product, process, or service by trade name, trademark, manufacturer, or otherwise, does not necessarily constitute or imply its endorsement, recommendation, or favoring by the United States Government or any agency thereof. The views and opinions of authors expressed herein do not necessarily state or reflect those of the United States Government or any agency thereof.

ORNL/TM-11701
Dist. Category UC-427

Fusion Energy Division

MERCIER STABILITY AND TRANSPORT PROPERTIES OF THE URAGAN-2M AND ATF TORSATRONS

N. Dominguez
B. A. Carreras
V. E. Lynch

J. S. Tolliver
Computing and Telecommunications Division
Martin Marietta Energy Systems, Inc.

V. E. Bykov
D. L. Grekov
A. A. Shishkin
Kharkov Institute of Physics and Technology
Kharkov, Ukraina, U.S.S.R.

Date published—February 1991

Prepared for the
Office of Fusion Energy
under Budget Activity No. AT 05 20 21 0

Prepared by the
OAK RIDGE NATIONAL LABORATORY
Oak Ridge, Tennessee 37831-6285
managed by
MARTIN MARIETTA ENERGY SYSTEMS, INC.
for the
U.S. DEPARTMENT OF ENERGY
under contract DE-AC05-84OR21400

MARTIN MARIETTA ENERGY SYSTEMS LIBRARIES

3 4456 0331054 8

CONTENTS

ABSTRACT v
I. INTRODUCTION 1
II. VACUUM MAGNETIC CONFIGURATIONS AND FINITE-BETA EQUILIBRIA 3
III. IDEAL MHD STABILITY 10
IV. NEOCLASSICAL TRANSPORT IN THE LOW-COLLISIONALITY REGIME 15
V. DISCUSSIONS AND CONCLUSIONS 24
ACKNOWLEDGMENTS 25
REFERENCES 26

ABSTRACT

The equilibrium, Mercier stability, and neoclassical transport (in the $1/\nu$ regime) properties of two $\ell = 2$ torsatrons, the Advanced Toroidal Facility (ATF) and URAGAN-2M, are compared. ATF and URAGAN-2M have 12 and 4 field periods, respectively. The two torsatrons have similar arrays of coils. Dipole and quadrupole magnetic fields can be used to improve transport at zero beta, but increasing beta tends to undo the optimization.

I. INTRODUCTION

The Advanced Toroidal Facility (ATF) [1] in operation at Oak Ridge National Laboratory and the URAGAN-2M [2–4] under construction at Kharkov Physics and Technology Institute are torsatrons with the same multipolarity number, $\ell = 2$. They differ in the number of toroidal field periods M, coil aspect ratio $A_c = R_0/a_c$, and helical coil winding law. The two devices have similar systems of poloidally symmetric coils that permit the variation of the magnetic configuration for testing their confinement properties. The main parameters for both devices are listed in Table I.

We evaluate the equilibrium and stability properties of URAGAN-2M using the techniques and numerical tools that were used in designing and evaluating the ATF configuration. For the standard URAGAN-2M configuration, with a minor radius of 12 cm, the plasma beta is limited by equilibrium. Values of $\beta_0 \approx 2\%$ are accessible. For an URAGAN-2M configuration with a plasma minor radius of 17 cm, we have found that values of peak beta up to about 1.5% are stable to Mercier modes. The results are for a fixed pressure profile; therefore, they should be considered only lower bounds for the plasma performance.

From the analysis of finite-beta configurations, the $B \equiv |\vec{B}|$ spectrum is calculated and used for evaluation of the transport properties of both devices in the so-called $1/\nu$ regime [5]. It is interesting to compare the confinement properties of the two torsatrons as well as those of different configurations in the same device. These comparisons lead to the definition of experimental tests of these confinement properties and of the basic transport theory.

TABLE I

Parameters of ATF and URAGAN-2M torsatrons

	R_0 (m)	a_c (m)	M	B_0 (T)
ATF	2.1	0.48	12	2.0
URAGAN-2M	1.7	0.445	4	2.0

The remainder of the paper is organized as follows. In Sec. 2, the vacuum magnetic configurations used for these studies are described, as is the numerical modeling. These configurations are the input used for the three-dimensional (3-D) equilibrium calculations. The stability properties of the URAGAN-2M equilibria are presented in Sec. 3 and compared with the results for the ATF configuration obtained in Ref. [6]. The neoclassical transport coefficients are calculated in Sec. 4, and in Sec. 5 a discussion of these results and the conclusions are presented.

II. VACUUM MAGNETIC CONFIGURATIONS AND FINITE-BETA EQUILIBRIA

The basic magnetic configuration of URAGAN-2M and its magnetic vacuum field properties are described in Refs. [2–4, 7]. Here, we discuss the modeling of the vacuum field that has been used as input to the equilibrium and stability calculations.

The URAGAN-2M helical coil system is characterized by two helical coils wound on a torus of major radius $R_c = 1.7$ m, with a winding law

$$\varphi = \frac{\ell}{M}(\theta - \alpha \sin\theta - \gamma \sin 2\theta) \quad . \tag{2}$$

Here, φ and θ are the geometric toroidal and poloidal angles, respectively. The winding law modulation parameters have already been fixed, and their values are $\alpha = 0.2618$ and $\gamma = -0.0171$. Because the URAGAN-2M helical coils span, poloidally, a large angle and each coil is split in two, we had to use multiple filaments to model each coil. It was found [4] that an efficient representation was achieved by using three filaments for each half of a helical coil. The central filament follows the winding law given in Eq. (1). The other two filaments ae shifted poloidally an angle of $\pm 12°$. The poloidally symmetric coil system is characterized by a system of six pairs of circular coils, each of which has been modelled by a single filament. The URAGAN-2M device also has 16 toroidal field coils that have been modelled by 2 parallel filaments for each coil. The filament model used for the present calculations is shown schematically in Fig. 1.

In characterizing the different URAGAN-2M configurations, let us consider the parameters $K_\varphi = B_{\varphi,h}/B_0$ and $B_\perp/B_0$. Here, $B_{\varphi,h}$ is the φ component of the helical field at the major radius position $R = R_0$, $B_0 = B_{\varphi,t} + B_{\varphi,h}$ is the average φ component of the total magnetic field at R_0, and $B_\perp$ is the transverse magnetic field correction at R_0.

The present results for the vacuum magnetic surfaces confirm the previous results [2–4]. For a configuration with $K_\varphi = 0.375$ and $B_\perp/B_0 = 0.028$, the standard configuration, the last closed flux surface (LCFS) has an average radius $a = 12.7$ cm. Outside the radius there is a chain of islands resonant with $\iota = 4/6$ [3]. In Ref. [4], a way was found to eliminate this chain of islands and increase the average radius of the plasma. The magnetic islands are eliminated by changing the coefficient γ in the helical coil winding law [4] using a method similar to that of Cary and Hanson [8]. This improved configuration is not considered further in this paper.

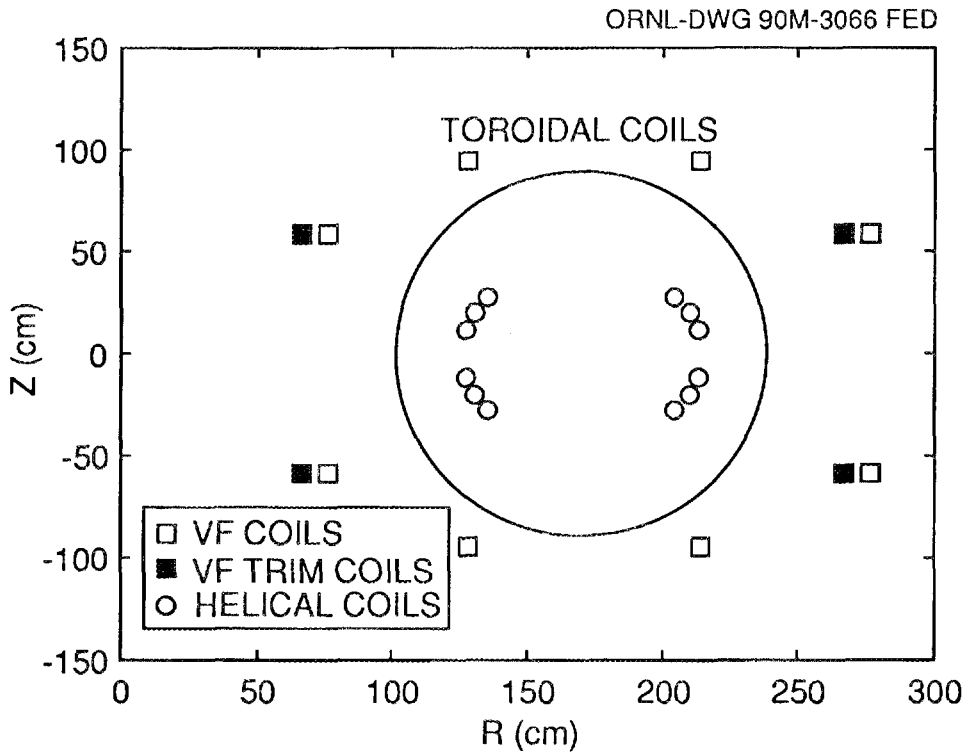

Fig. 1. Coil model used for URAGAN-2M vacuum magnetic field calculations.

A second configuration, which we study in detail, corresponds to $K_\varphi = 0.375$ and $B_\perp/B_0 = 0.015$ with an average radius for the LCFS of $\alpha = 17.0$ cm. The standard configuration is such that the LCFS does not intersect the vacuum vessel of the device. For the second configuration, because of the larger minor radius of the LCFS, the URAGAN-2M vacuum vessel should be modified. Therefore, it is of practical importance to evaluate the merits of these two configurations. Hereafter, we use the value of $B_\perp/B_0$ to identify these configurations.

The vacuum field rotational transform, ι, and the specific volume, V', profiles for these two configurations are plotted in Fig. 2. The standard configuration is characterized by a low-shear profile with a rotational transform $\iota = 0.57$ and a broad magnetic well. The configuration with $B_\perp/B_0 = 0.015$ has shear at the edge, with a rotational transform going from 0.5 to 0.7. As a consequence, it has the typical edge magnetic hill characteristic of most torsatron configurations.

The 3-D equilibria for the two URAGAN-2M configurations have been obtained with the VMEC code [9]. We have considered only zero-current equilibria with a parabolic pressure profile,

$$P = P_0(1 - \Psi)^2 \quad . \tag{2}$$

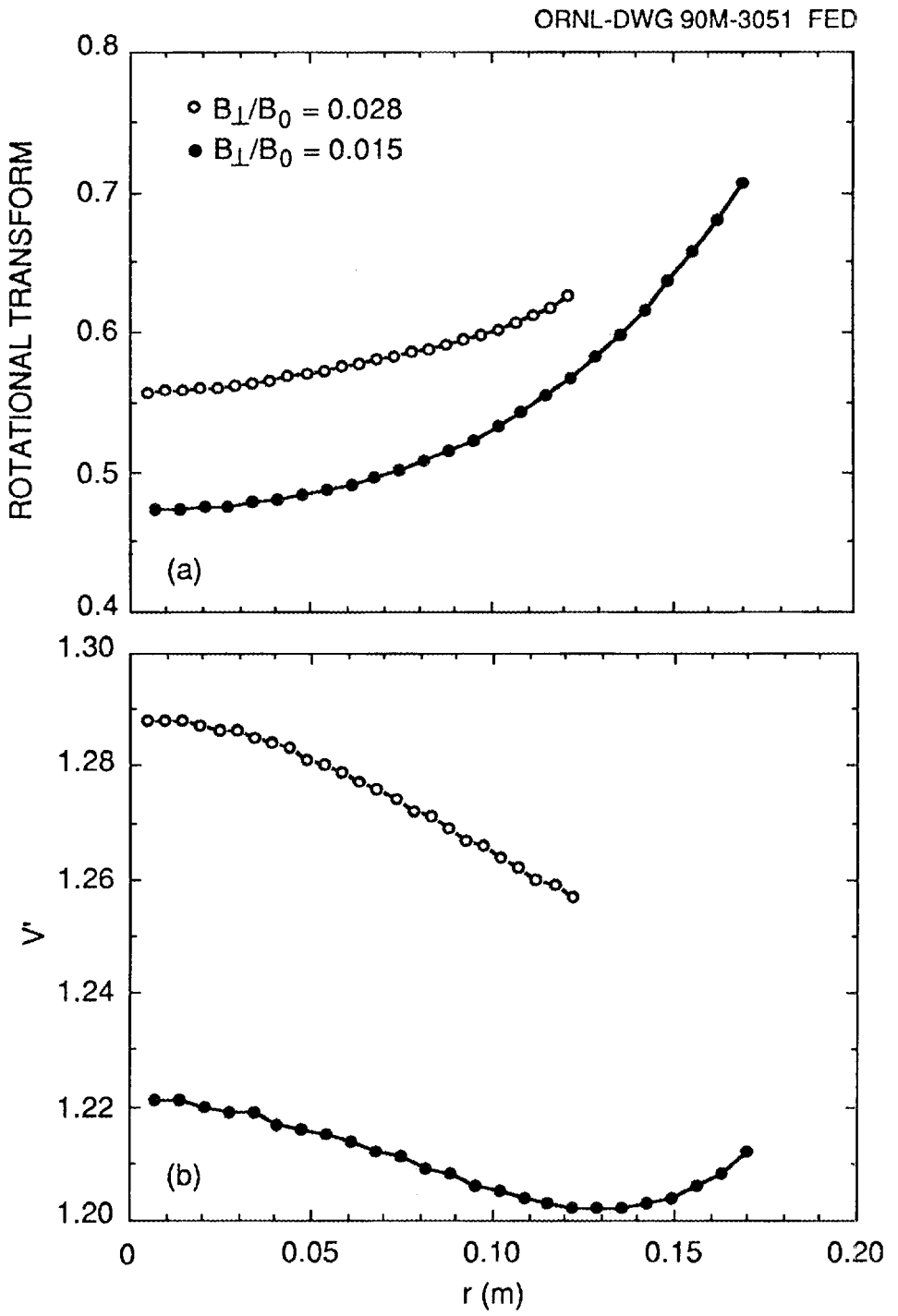

Fig. 2. Vacuum rotational transform and V' profiles for the two URAGAN-2M configurations discussed in the text.

Here, Ψ is the poloidal flux normalized to 1 at the plasma boundary. Both fixed and free boundary equilibria have been considered. For fixed boundary equilibria, the boundary is determined as a Fourier expansion of the R and Z coordinates in the poloidal and toroidal angles. The boundary is calculated by using the DESCUR code [10] to fit the LCFS obtained with the magnetic field line following code. For URAGAN-2M, we have used harmonics with poloidal mode numbers m such as $0 \leq m \leq 5$ and toroidal mode numbers n such as $-7M < n < 7M$, where $M = 4$ is the number of toroidal field periods. In total, 68 harmonics are needed to specify the boundary with an rms value of 8×10^{-3}. This is accurate enough for the zero-beta equilibria to reproduce the rotational transform and V' profiles obtained with the field line following code. In these calculations, equally spaced grids of 31 and 61 radial grid points were used.

The equilibrium results for both URAGAN-2M configurations are summarized in Table II. In this table, β_0 is the peak beta value, and Δ_T is the normalized toroidal magnetic shift, which has been defined as the magnetic axis position at $\beta \neq 0$ minus its position at $\beta = 0$ divided by the average minor radius. The magnetic axis shifts for both configurations are plotted in Fig. 3. Examples of the flux surfaces for both configurations are shown in Fig. 4.

TABLE II

Fixed boundary equilibrium results for the two URAGAN-2M configurations considered in this paper

$B_\perp/B_0 = 0.028$		$B_\perp/B_0 = 0.015$	
$\beta_0(\%)$	$\Delta_T(\%)$	$\beta_0(\%)$	$\Delta_T(\%)$
0.0	0.0	0.0	0.0
1.04	5.3	0.85	3.7
2.02	11.8	2.74	17.1
2.12	13.1	5.8	34.9
4.86	27.5	7.59	41.8
6.74	38.7		

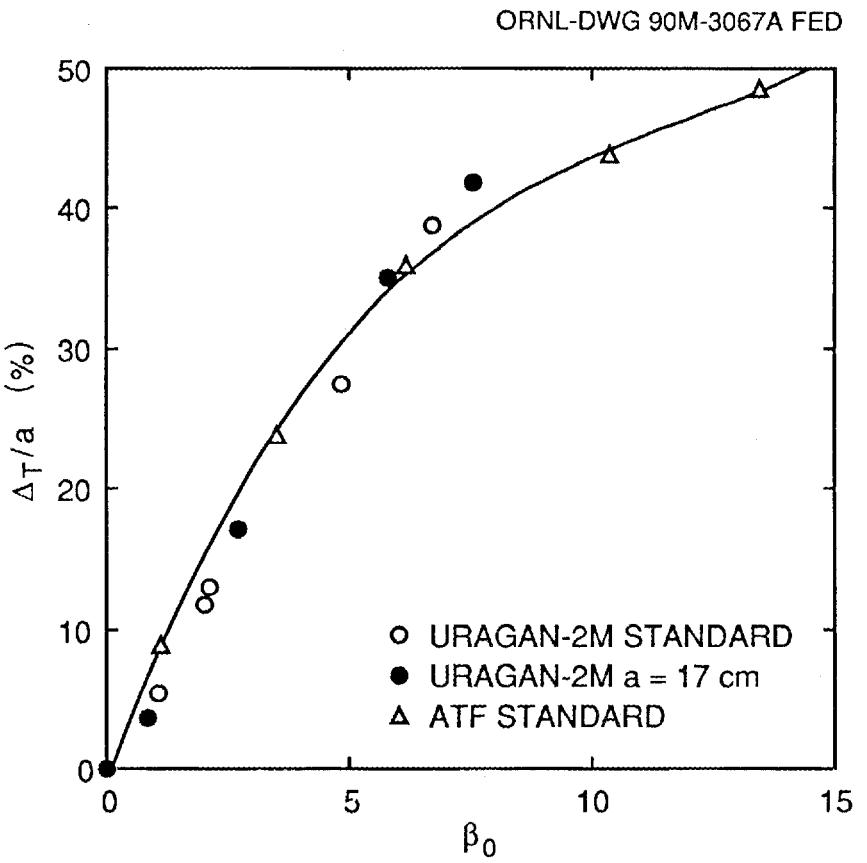

Fig. 3. Magnetic axis shift with beta for the two URAGAN-2M configurations and the standard ATF configuration.

Taking $\Delta_T \approx 50\%$ as a measure of the equilibrium beta limit, we find, by fitting the calculated Δ_T values and extrapolating to 50% shift, that both configurations have a peak beta limit of $\beta_0 \approx 9\%$. Because of the low transform and shear of the standard configuration, the finite-beta distortion of the rotational transform profile introduces in the plasma low-m resonances that interfere with the numerical convergence of the 3-D equilibrium code. For $\beta_0 \approx 2\%$ and the pressure profile of Eq. (1), it is not possible to get a well-converged zero-current equilibrium. The problem seems to be associated with the $\iota = 0.6$ surface coinciding with a zero-shear region. These results probably indicate that for the standard configuration the beta limit is governed by the process of island formation. For higher β_0 values the shear, both positive and negative, increases, and a well-converged equilibrium is found. The use of the quadrupole field to control the rotational transform [11] can be important for accessing high-beta equilibria for the standard configuration.

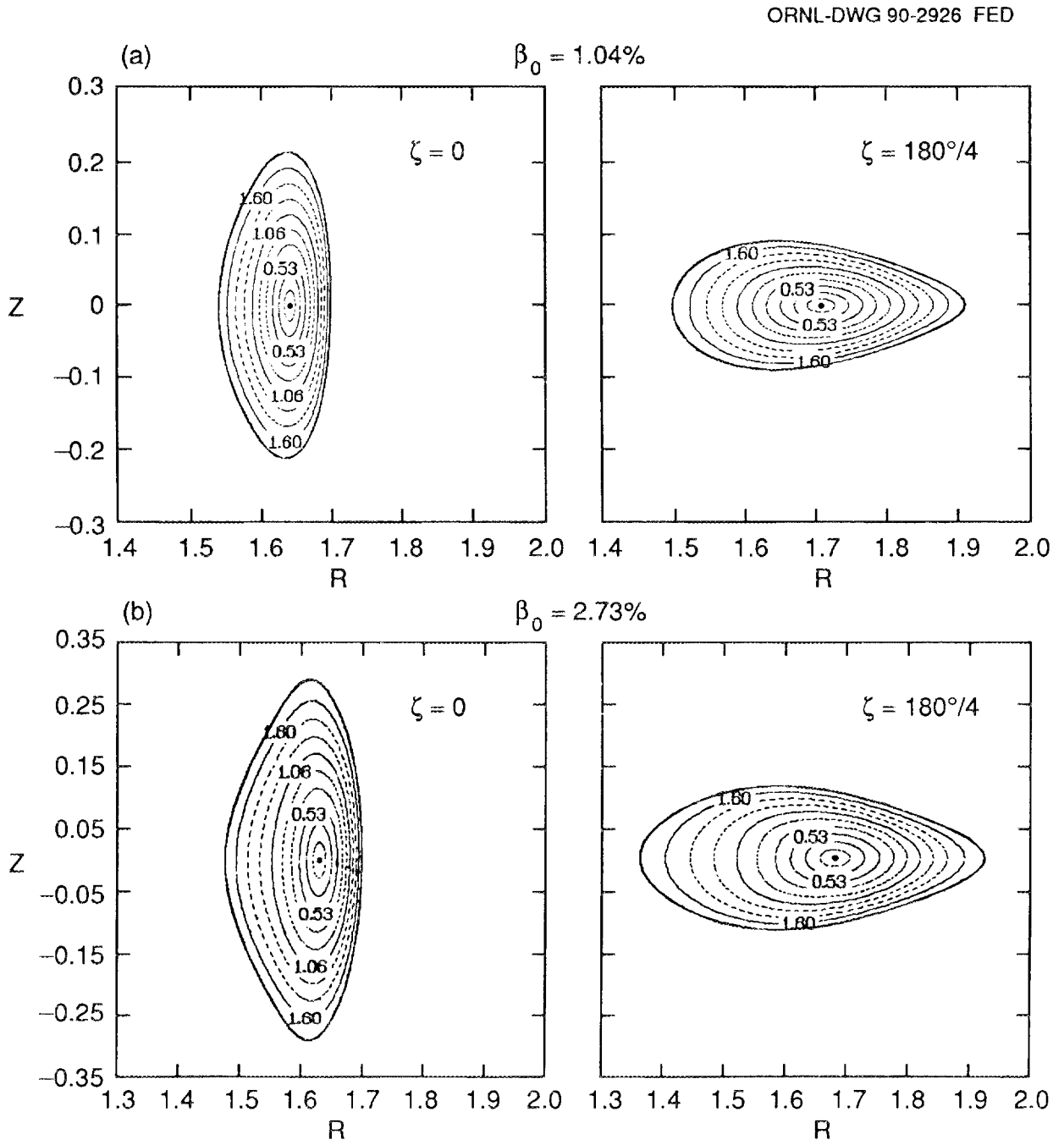

Fig. 4. Magnetic flux surfaces for (a) $B_\perp/B_0 = 0.028$ with $\beta_0 = 1.04\%$ and (b) $B_\perp/B_0 = 0.015$ with $\beta_0 = 2.73\%$ URAGAN-2M configurations.

For the same pressure profile and using the same method as for the URAGAN-2M configurations, the ATF equilibrium beta limit is $\beta_0 \approx 15\%$. This higher beta limit is a consequence of the higher rotational transform at the edge, $\iota(a) \approx 1$, in the ATF device. However, the slope of Δ_T as a function of β_0 is not as different for the two devices as the values of aspect ratio and ι would suggest, because of the lower value of $\langle J_{\parallel}^2\rangle^{1/2}/\langle|\vec{J}_{\perp}|^2\rangle^{1/2}$ for URAGAN-2M (Fig. 5).

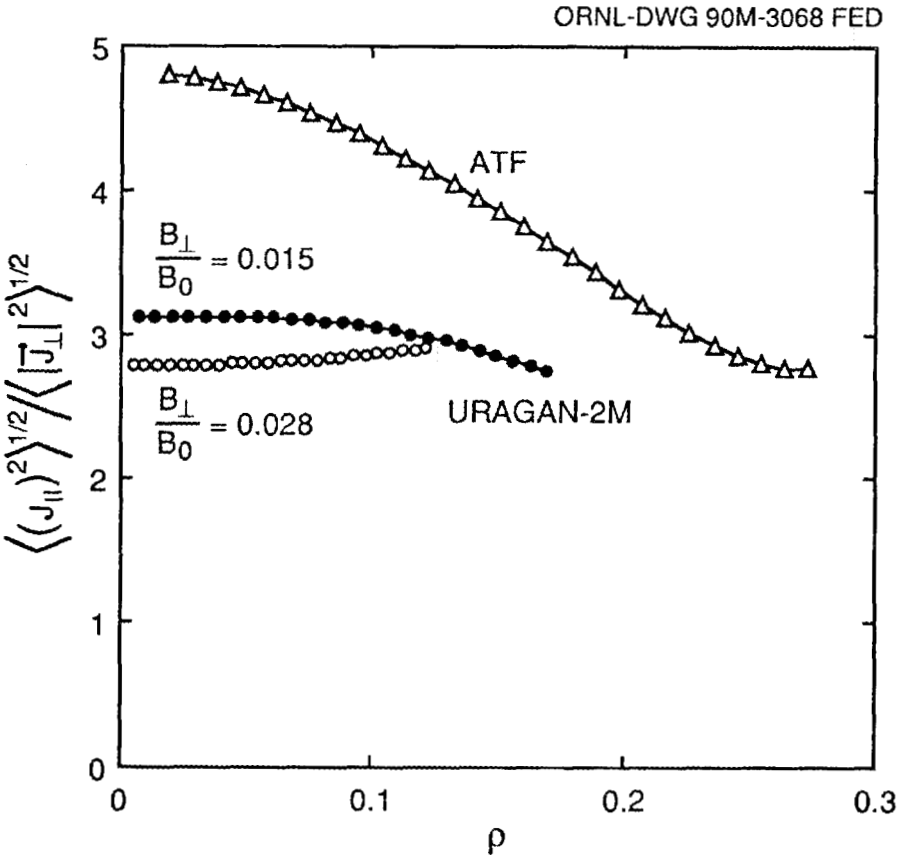

Fig. 5. Radial profile of $\langle(J_{\parallel})^2\rangle^{1/2}/\langle|\vec{J}_{\perp}|^2\rangle^{1/2}$ for the two URAGAN-2M configurations compared with the ATF profile.

III. IDEAL MHD STABILITY

We have limited our ideal MHD stability studies to testing the Mercier criterion [12] for the two URAGAN-2M configurations. The Mercier criterion can be written as [13]

$$D_M = D_S + D_I + D_W + D_G > 0 \quad , \tag{3}$$

with D_S the shear, D_W the magnetic well, D_I the net current, and D_G the geodesic curvature. The condition $D_M > 0$ implies stability. Here,

$$D_S = \frac{(\Psi''\Phi')^2}{4}\frac{s}{\iota^2\pi^2} \ , \tag{4}$$

$$D_W = \frac{s}{\iota^2\pi^2}\iint g\ d\theta\ d\zeta \frac{B^2}{g^{ss}}\frac{dp}{ds}\left(V'' - \frac{dp}{ds}\iint \frac{g\ d\theta\ d\zeta}{B^2}\right) \ , \tag{5}$$

$$D_I = \frac{s}{\iota^2\pi^2}\left[\iint g\ d\theta\ d\zeta \frac{B^2}{g^{ss}}\Psi'' I' - (\Psi''\Phi')\iint \frac{g(\vec{J}\cdot\vec{B})d\theta\ d\zeta}{g^{ss}}\right] \ , \tag{6}$$

$$D_G = \frac{s}{\iota^2\pi^2}\left\{\left[\iint \frac{g(\vec{J}\cdot\vec{B})d\theta\ d\zeta}{g^{ss}}\right]^2 - \left[\iint \frac{g(\vec{J}\cdot\vec{B})d\theta\ d\zeta}{g^{ss}B^2}\right]\left(\iint g\ d\theta\ d\zeta \frac{B^2}{g^{ss}}\right)\right\} \ , \tag{7}$$

where $\vec{J}$, $\vec{B}$, and P are the equilibrium plasma current, magnetic field, and plasma pressure, respectively. The quantity B is the magnitude of the magnetic field. A flux coordinate system is used for which g is the Jacobian, and the flux surface label s is defined as $s = 2(\Phi/2\pi)$, where Φ is the magnetic toroidal flux. An average radius for each magnetic surface is defined by $\rho = \sqrt{s}$. In Eqs. (4)–(7), a prime denotes the derivative with respect to the flux label s.

The surface average of the Jacobian, $V' = \int\int g\ d\theta\ d\zeta$, is the specific volume that gives a measure of the magnetic well or hill of the configuration. The net toroidal current enclosed by a flux surface is I, and the metric element that appears in the denominator of the integrand in Eqs. (5)–(7) is $g^{ss} = \nabla s \cdot \nabla s$. All four of the terms in Eq. (3) play a role in determining the stability of a given configuration. They change with beta in different ways, depending on the configuration and the pressure profile.

For the standard configuration, the dominant terms determining the Mercier stability are the magnetic well contribution D_W and the geodesic curvature D_G. Because the shear is low, it effectively does not contribute to the Mercier criterion (Fig. 6). For the range of beta values analyzed, the magnetic well contribution

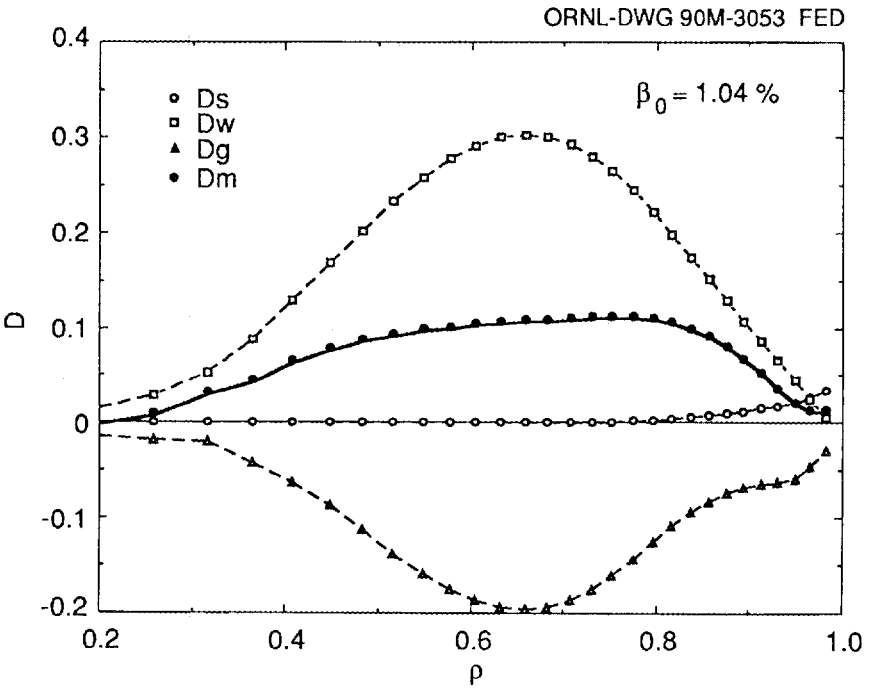

Fig. 6. Contributions to Mercier criterion for the $B_\perp/B_0 = 0.028$ configuration for $\beta_0 = 1.04\%$.

dominates the geodesic curvature contribution. For this configuration, the value of beta is limited by equilibrium convergence, not by stability.

The configuration with a larger minor radius, the $B_\perp/B_0 = 0.015$ configuration, has stability properties different from those of the standard configuration. This is illustrated in Fig. 7, where the different contributions to the Mercier criterion are plotted for $\beta_0 = 2.7\%$. The contribution of the magnetic well is not positive over the whole radial range, and near the boundary it is negative because of the magnetic hill. Moreover, the shear contribution compensates for the magnetic hill at the edge. The main stability problem comes from the geodesic curvature at the $\iota = 1/2$ resonance, which makes D_M negative around the radius $\rho = 0.4a$ and near the edge ($\rho \sim 0.8a$) because the shear contribution is not large enough to compensate for the magnetic hill. The stability beta limit is $\beta_0 \simeq 1.5\%$.

To illustrate the effects of finite beta on the rotational transform, we have plotted, in Fig. 8, the rotational transform as a function of radius for different values of beta for equilibria corresponding to the configuration with $B_\perp/B_0 = 0.015$. The Mercier stability properties of this configuration are similar to those of ATF [6], as seen in Fig. 9, where the stability boundaries are plotted for the URAGAN-2M

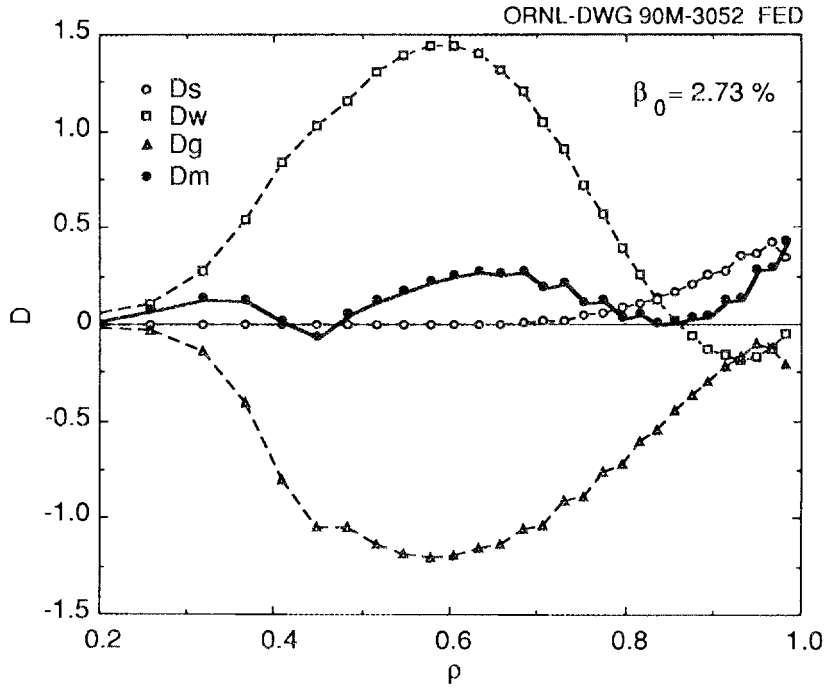

Fig. 7. Contributions to Mercier criterion for the $B_\perp/B_0 = 0.015$ configuration for $\beta_0 = 2.73\%$.

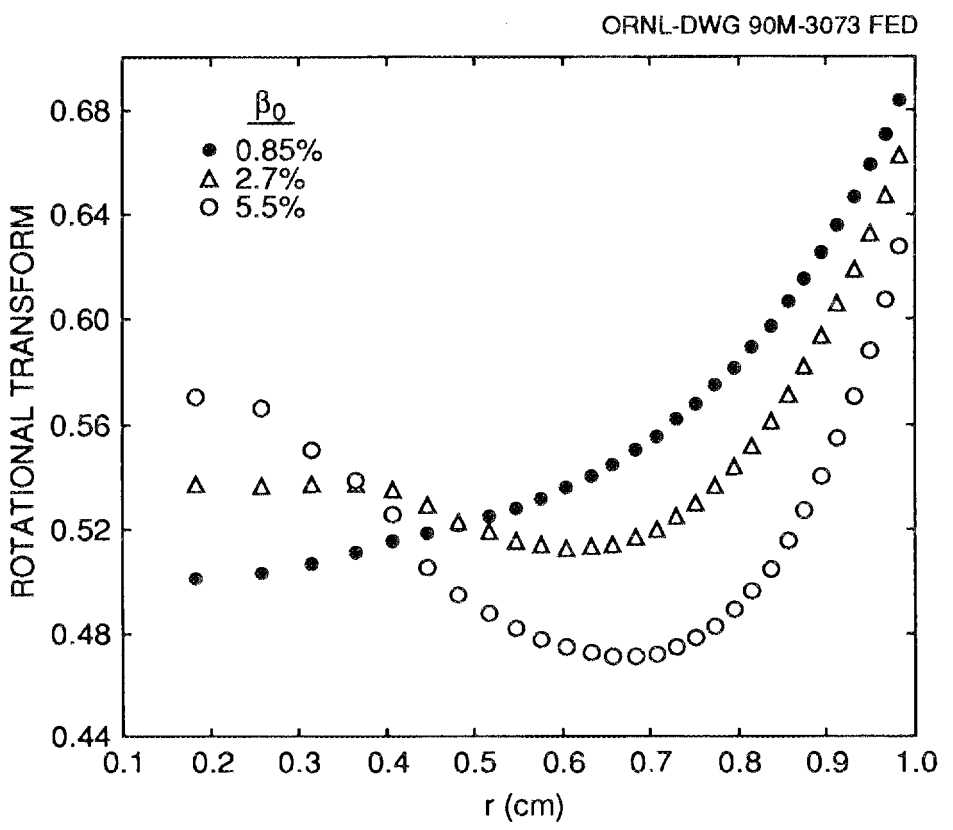

Fig. 8. Rotational transform as a function of radius for different values of beta for the configuration with $B_\perp/B_0 = 0.015$.

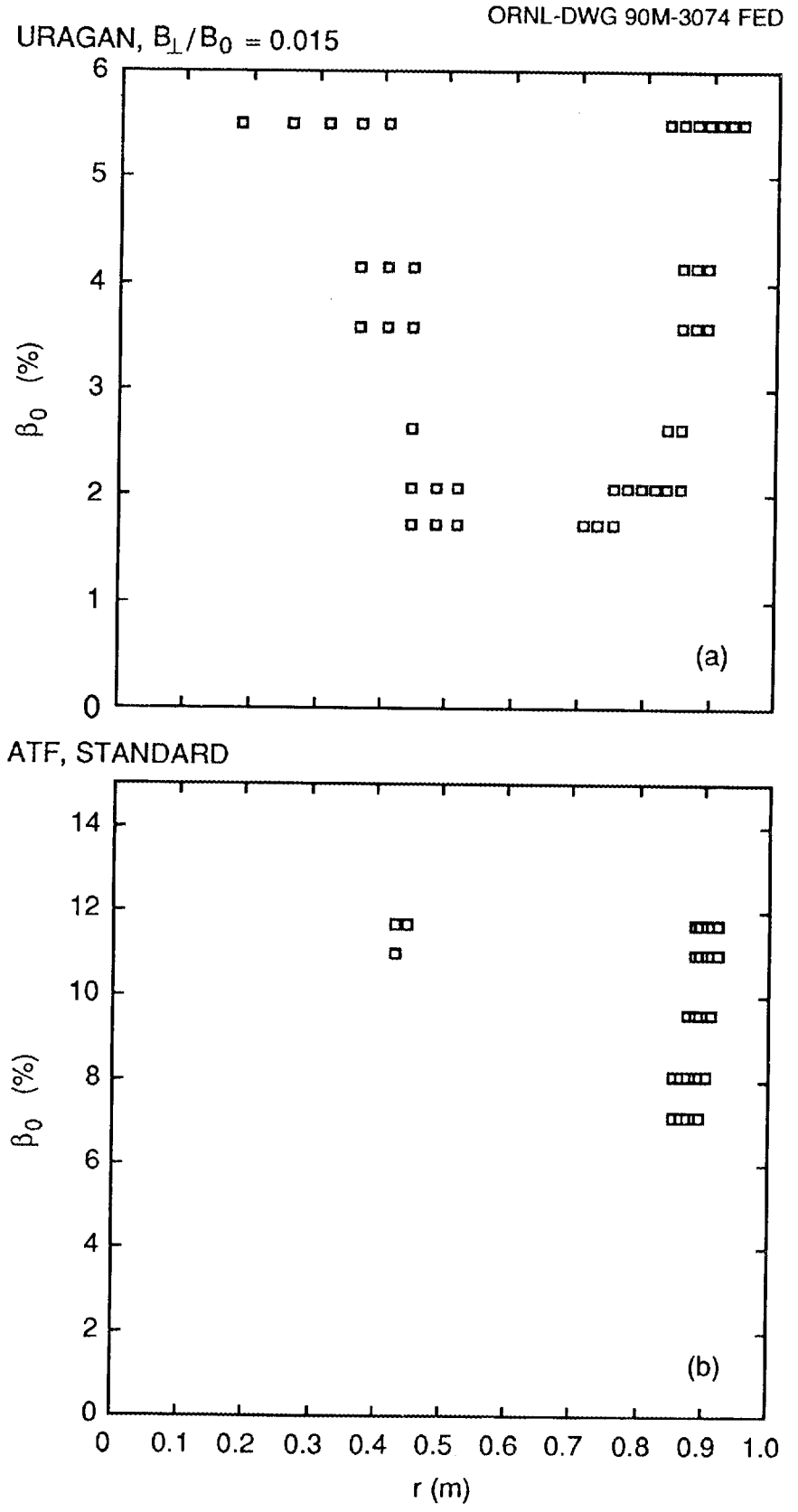

Fig. 9. Stability boundaries for the URAGAN-2M configuration with $B_\perp/B_0 = 0.015$ and the standard ATF configuration.

configuration with $B_\perp/B_0 = 0.015$ and the ATF standard configuration. Therefore, it is plausible that pressure profiles exist for URAGAN-2M that allow stable operation at higher peak beta values for this configuration. The rotational transform profile distortion with beta is also a very important effect for this configuration. The use of the quadrupole field to control the transform [11] could help in extending the range of stable operation for this configuration.

IV. NEOCLASSICAL TRANSPORT IN THE LOW-COLLISIONALITY REGIME

A main concern for stellarator confinement is the level of losses in the $1/\nu$ regime that are not affected by the electric field effects. The particle flux in the $1/\nu$ regime has been calculated in Refs. [5, 7, 14, 15] for multiple-helicity stellarators. When only toroidal ripple ϵ_t and helical ripple ϵ_h are considered, the particle flux in the $1/\nu$ regime scales as $\epsilon_h^{3/2}\epsilon_t^2/r^2$. The presence of other harmonics, introduced by the geometry of the magnetic field, changes this scaling. Here, we consider how these changes affect the configurations under study.

For a given device, there are some ways to change the geometric factors of transport coefficients. One is to use a dipole magnetic field to displace the vacuum magnetic axis from the geometric axis of the chamber. Another is to use a magnetic quadrupole field to change the shape of the magnetic surfaces. It is also important to take into account the changes caused by beta. In many cases, they tend to offset the improvements in confinement made for the vacuum fields [15, 16]. All changes of shape and position of the magnetic surfaces cause changes in the magnetic field modulation, and they influence the charged particle motion and transport.

We have compared some types of magnetic configurations for ATF and URAGAN-2M from the viewpoint of neoclassical transport in the $1/\nu$ regime. In the $1/\nu$ regime, the neoclassical particle flux is proportional to the product of plasma quantities times the geometric factor D,

$$\Gamma \propto -\frac{D}{m_s^{7/2}\omega^2 r_0^2}\int_0^\infty dW \frac{W^{5/2}}{\nu}\frac{\partial f_M}{\partial r} \quad , \tag{8}$$

where m_s is the mass of the species, ω is the Larmor frequency, ν is the collision frequency, and the integral is on the energy over a Maxwellian distribution f_M.

The expression for the energy flux is similar, except that the exponent of the energy W in the integrand is $7/2$. For the geometric factor D, we have used an analytical expression [5, 14, 15]

$$D = \frac{\epsilon_h^{3/2}\epsilon_t^2}{r^2}\left[\gamma_1 - \frac{\epsilon_h}{\epsilon_t}\gamma_2 + \left(\frac{\epsilon_h}{\epsilon_t}\right)^2 \gamma_3\right] \quad , \tag{9}$$

where γ_1, γ_2, and γ_3 are functions of the ratios $\epsilon_{1\pm1}/\epsilon_h$ and $\epsilon_{1\pm2}/\epsilon_h$, where $\epsilon_{1\pm1}, \epsilon_{1\pm2}$ are the amplitudes of the poloidal satellite harmonics.

The results are plotted in Figs. 10–13. All values in the figures are normalized. To obtain the geometric factor D in dimensional form, the values in the plots must be multiplied by 10^{-7} cm^{-2}.

For ATF, we can change the shape of the magnetic surfaces by applying a quadrupole field. In this way, the geometric factor D of the transport coefficients in the $1/\nu$ regime can be controlled. As a measure of the applied quadrupole field, we use the ratio I_m of the current in the mid-vertical field (VF) coil to the current in the helical coils. The value of D for $I_m = -0.13$ is 2 times smaller than that for the standard configuration ($I_m = 0$) and almost 4 times smaller than that for the $I_m = 0.13$ configuration. At the center of the plasma column, the difference between two extreme cases is approximately 2 (Figs. 10–12, open circles).

In the presence of plasma ($\beta \neq 0$), the factor D increases. At the inner half of the plasma, this increase is larger for the configuration with $I_m < 0$ than for the one with $I_m > 0$. The geometric coefficient D becomes equal for both configurations ($I_m = \pm 0.13$) at $\beta_0 = 6\%$. At finite beta, the improvement obtained by changing the quadrupole field is lost [16]. Therefore, the use of quadrupole fields is not the best way of optimizing transport at the center of the plasma cross section.

At the plasma boundary and for the fixed boundary equilibrium, the value of D remains close to that of the vacuum configuration. For free boundary equilibria and for $\beta_0 \approx 6\%$, the value of D for the $I_m = -0.13$ configuration is lower by a factor of 6 than that for the $I_m = 0.13$ configuration near the plasma edge, but both configurations have a larger geometric factor than the standard configuration (Fig. 13). Of course, in a free boundary calculation, control of the LCFS plays an important role, and some of the observed effects can be caused by not having adjusted the vertical field accurately enough. The role of the dipole field on the geometric factor is illustrated in Fig. 14. When the vacuum magnetic axis is shifted inward ($R_0 = 205$ cm), the value of D is smaller, almost 6 times, than when the vacuum magnetic axis is shifted outward ($R_0 = 215$ cm) and 3 times smaller than in the standard configuration ($R_0 = 210$ cm).

Similar results have been obtained for URAGAN-2M vacuum magnetic fields [7]. For fixed boundary equilibria, increasing the plasma pressure up to about 5% causes D to increase by a factor of almost 2 at half the plasma radius (Figs. 15 and 16). Changing the URAGAN-2M configuration from $B_\perp/B_0 = 0.015$ to $B_\perp/B_0 = 0.028$ does not lead to noticeable changes in D (Fig. 17).

For free boundary equilibria, we consider an URAGAN-2M for which the plasma radius goes up to $a_0 \leq 25$–27 cm. This configuration can be obtained in the new

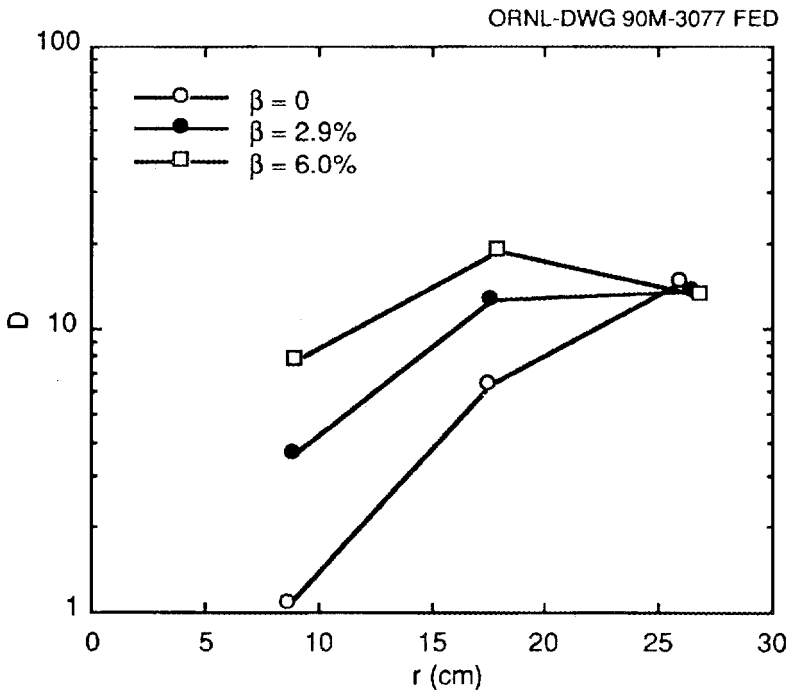

Fig. 10. Geometric factor D for $I_m = -0.13$ ATF configuration for $\beta_0 = 0$ (circles), $\beta_0 = 2.9\%$ (triangles), and $\beta_0 = 6\%$ (squares) fixed boundary equilibria.

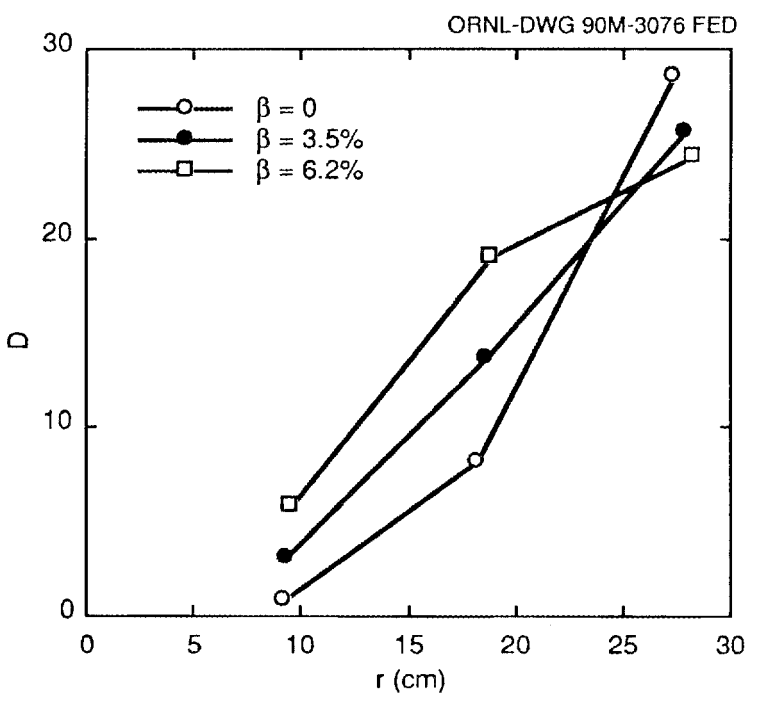

Fig. 11. Geometric factor D for the standard ATF configuration for $\beta_0 = 0$ (circles), $\beta_0 = 3.5\%$ (triangles), and $\beta_0 = 6.2\%$ (squares) fixed plasma boundary.

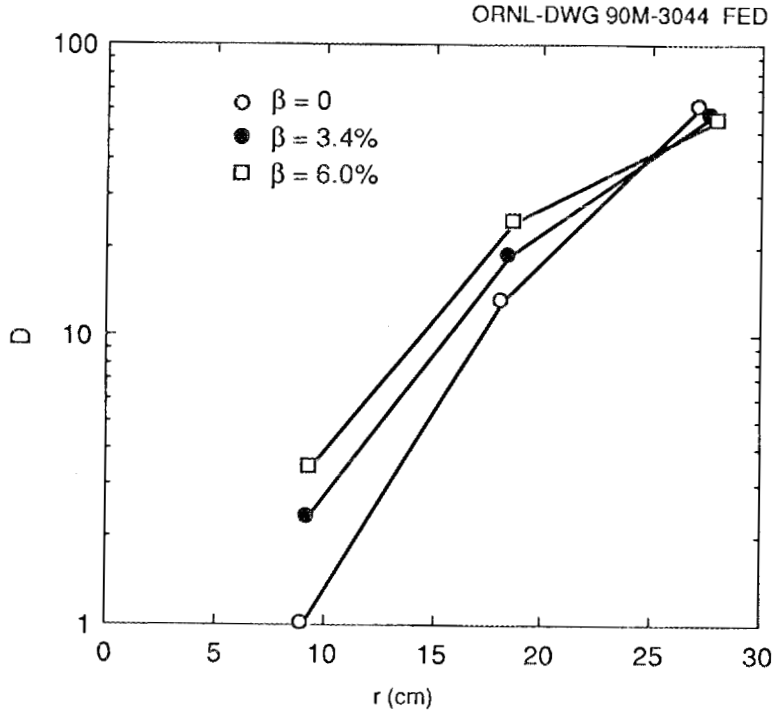

Fig. 12. Geometric factor D for $I_m = 0.13$ ATF configuration for $\beta_0 = 0$ (circles), $\beta = 3.4\%$ (triangles), and $\beta_0 = 6\%$ (squares) fixed plasma boundary.

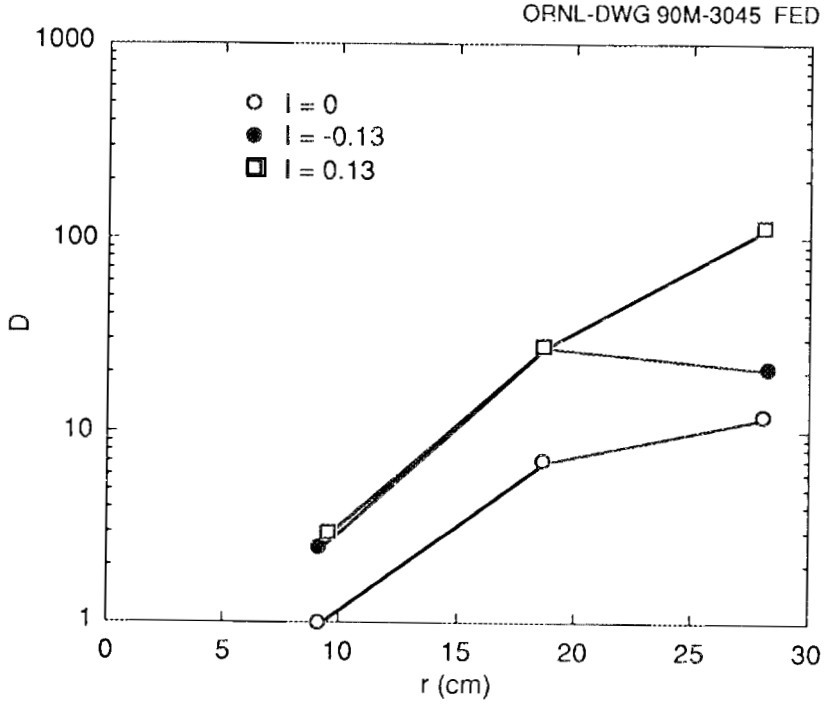

Fig. 13. Geometric factor D for $I_m = -0.13$ (circles), $I_m = 0$ (triangles), and $I_m = 0.13$ (squares) ATF configurations for $\beta_0 = 6\%$ free boundary equilibria.

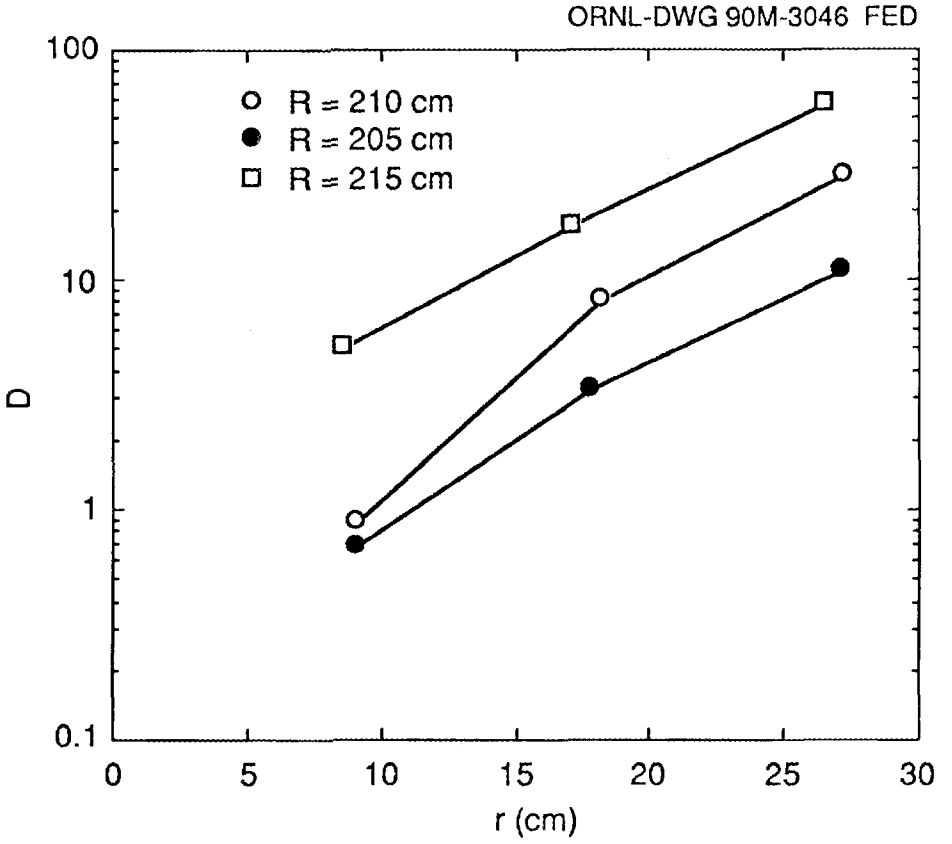

Fig. 14. Geometric factor D for the vacuum magnetic field ATF configuration with $R_0 = 215$ cm (triangles), $R_0 = 210$ cm (squares), and $R_0 = 205$ cm (circles).

modification of URAGAN-2M with profiled vacuum chamber. For this configuration, the value of D at the plasma edge is close to the values obtained for ATF. The fact that the value of D in URAGAN-2M is not smaller than in ATF for the same plasma size warrants some comment. For the same magnetic surface radius, the helical component ϵ_h is the same for both configurations [7]. The toroidal component ϵ_t is somewhat larger in URAGAN-2M than in ATF. When toroidal satellites are not taken into account, the geometric factor is smaller in ATF than in URAGAN-2M. URAGAN-2M is characterized by a positive sign of the nearest toroidal sidebands. This is a consequence of the helical winding modulation, which localizes the helical ripple more on the outside than on the inside of the torus. This modulation of the magnetic field is not favorable to trapped particle confinement. In this situation, the particle orbits have larger deviations from the magnetic surfaces. The ATF winding law has no modulation, which implies that the nearest sidebands

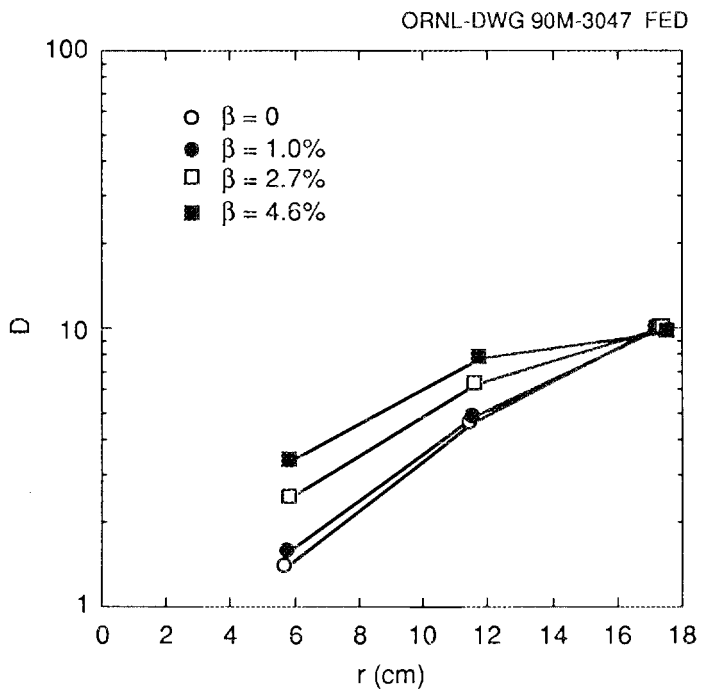

Fig. 15. Geometric factor D for the $B_\perp/B_0 = 0.015$ URAGAN-2M configuration for $\beta_0 = 0$ (open squares), $\beta_0 = 1\%$ (triangles), $\beta_0 = 2.7\%$ (circles), and $\beta_0 = 4.6\%$ (solid squares) fixed boundary equilibria.

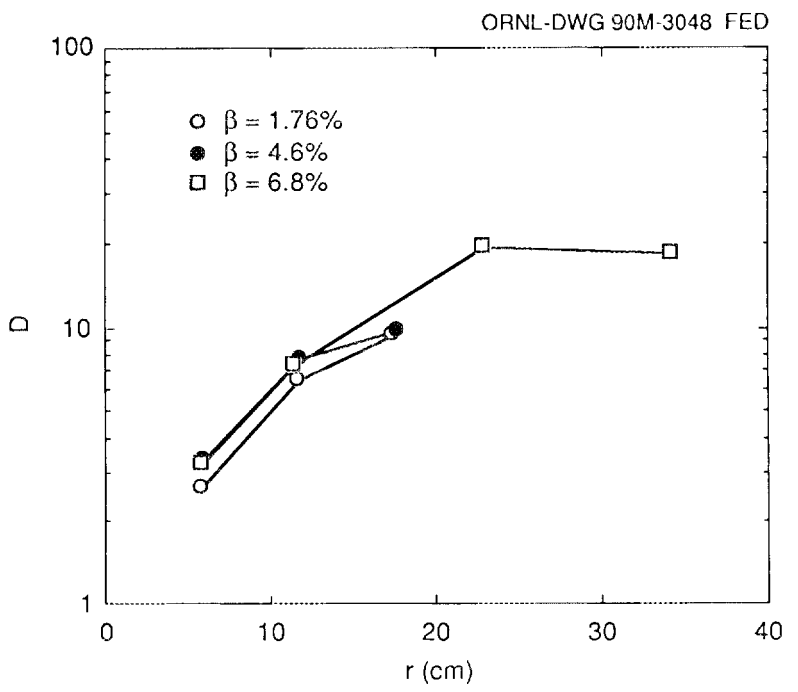

Fig. 16. Geometric factor D for the $B_\perp/B_0 = 0.015$ URAGAN-2M configuration for $\beta_0 = 1.5\%$ (triangles), $\beta_0 = 4.6\%$ (squares), and $\beta_0 = 6.8\%$ (circles) free boundary equilibria.

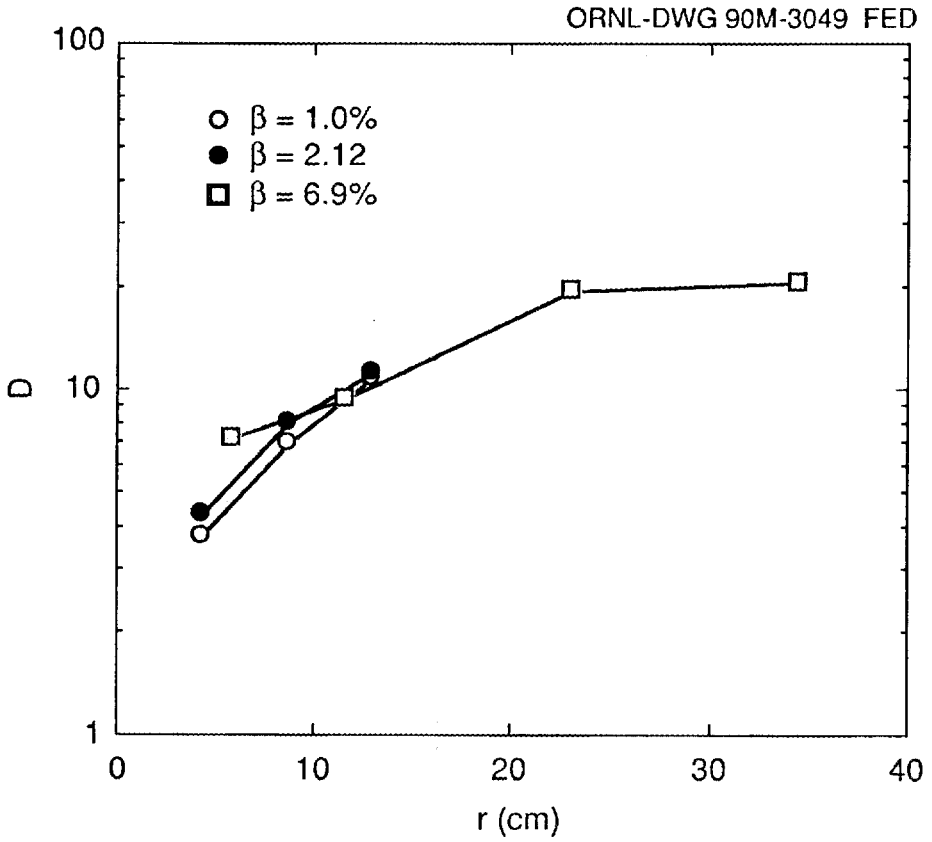

Fig. 17. Geometric factor D for the $B_\perp/B_0 = 0.028$ URAGAN-2M configuration for $\beta_0 = 1\%$ (squares), $\beta_0 = 2\%$ (triangles), and $\beta_0 = 7\%$ (circles) free boundary equilibria.

of helical harmonics have opposite signs. This form of B leads to smaller deviation of the trapped particle orbits from the magnetic surfaces. The effect of B on the trapped particle orbits can be visualized by plotting the minimum-B contours, which give a good description of the deeply trapped particle orbit topology [17], for the standard configurations of both devices (Fig. 18). In URAGAN-2M, there are no closed minimum-B contours inside the LCFS, indicating that all deeply trapped particles are lost. A similar plot is obtained for the $B_\perp/B_0 = 0.015$ URAGAN-2M configuration. In ATF, about 60% of the minimum-B contours are closed inside the LCFS. The plots in Fig. 18 are for the vacuum magnetic field configuration. At finite beta, the fraction of closed minimum-B contours decreases [16]. The loss of all deeply trapped particles for the URAGAN-2M configuration should be taken into consideration when choosing the plasma heating method for this device.

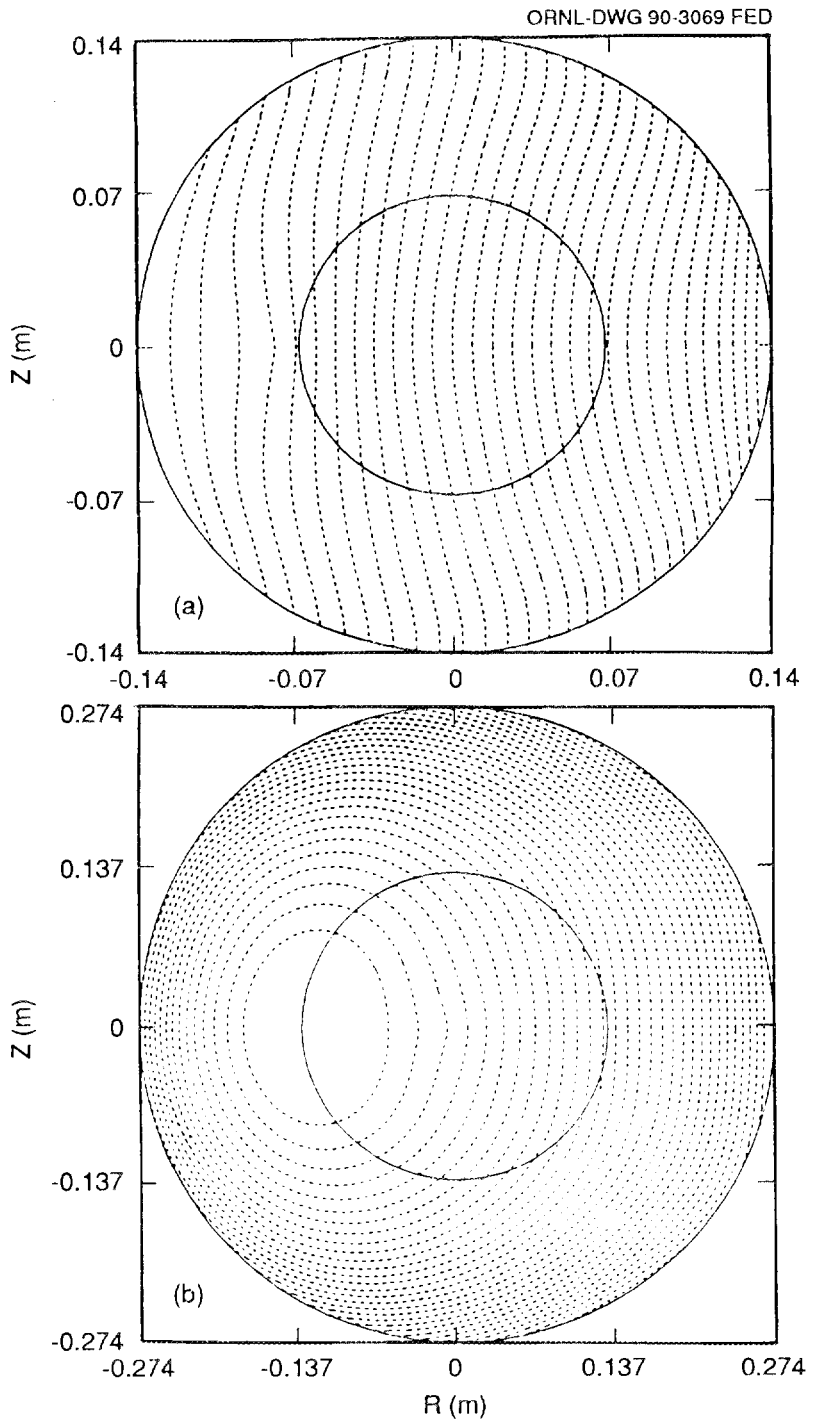

Fig. 18. Plot of the minimum-B contours for the standard configurations of (a) URAGAN-2M and (b) ATF in the plane ($\rho\cos\theta$, $\rho\sin\theta$). The circles are the $\rho = 1$ and $\rho = 0.5$ flux surfaces.

Finally, we have calculated the geometric factor of the bootstrap current in the low-collisionality regime for the two URAGAN-2M configurations. In the calculation, we have followed the semianalytical method described in Ref. [18]. The results are plotted in Fig. 19, and for the standard configuration they basically agree with the result of Ref. [4]. The value of G_b for both configurations is about the same and is about 0.5 in the region where the gradient of the pressure will probably peak.

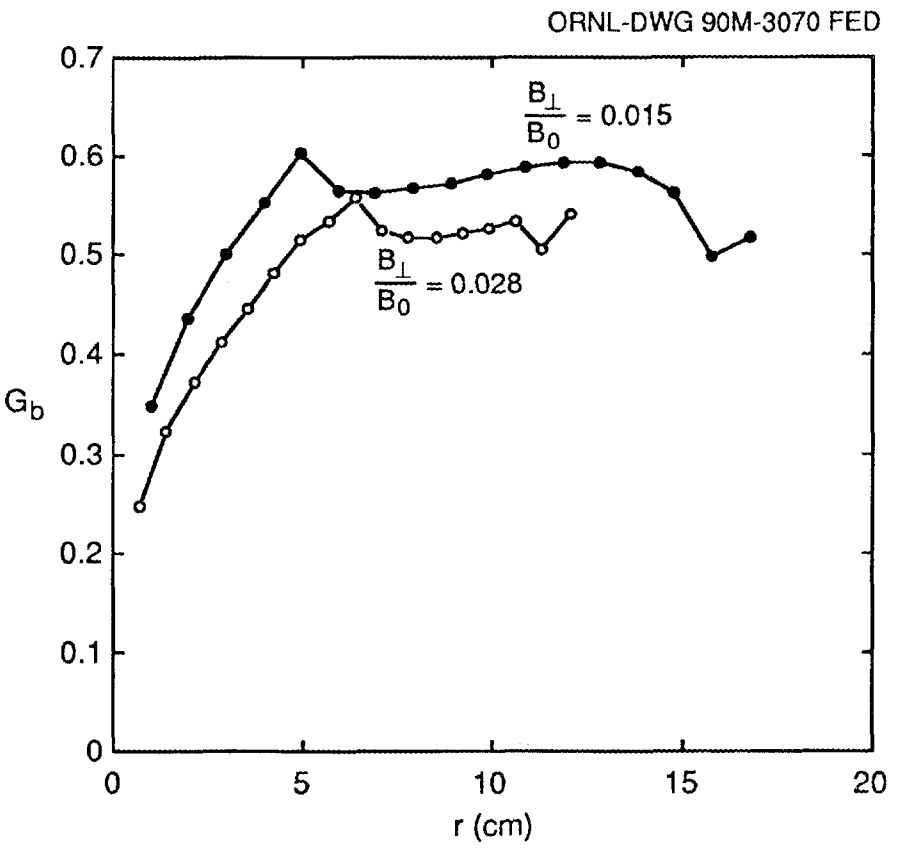

Fig. 19. Geometric factor for the bootstrap current in the low-collisionality regime for the URAGAN-2M configurations with (a) $B_\perp/B_0 = 0.028$ and (b) $B_\perp/B_0 = 0.015$.

V. DISCUSSIONS AND CONCLUSIONS

The evaluation of the equilibrium, Mercier stability, and neoclassical transport properties of URAGAN-2M, using the techniques and numerical tools used in designing and evaluating the ATF configuration, leads to the following results.

(1) For the standard URAGAN-2M configuration, with a minor radius of 12 cm, the plasma beta is limited by equilibrium. Values of $\beta_0 \approx 2\%$ are accessible. At higher beta, convergence problems in the 3-D equilibrium code are probably related to magnetic island formation. For the URAGAN-2M configuration with a plasma minor radius of 17 cm, we have found that values of peak beta up to about 1.5% are stable to Mercier modes. Since the calculations are for a fixed pressure profile, they should be taken as a lower bound for the operational parameters. The differences between the two configurations can be checked experimentally.

(2) Plasma equilibrium currents change the rotational transform profiles in such a way that regions with negative shear appear. For finite beta, the rotational transform may cross rational values that were avoided in designing the vacuum magnetic field configuration. External control of the rotational transform profile may be very important.

(3) The results for neoclassical transport in the $1/\nu$ regime show that the level of losses is the same for ATF and URAGAN-2M configurations with the same plasma radius. This result is valid for the vacuum magnetic field configuration as well as for finite-beta equilibria. The diffusion coefficient in ATF can be obtained as the diffusion coefficient for URAGAN-2M prolonged for the larger plasma radius. Therefore, in the $1/\nu$ regime and for the same magnetic field and plasma parameters (density and temperature), the ratio of confinement times in both devices depends only on the plasma size. Thus, it will be about three times larger in ATF than in URAGAN-2M.

(4) The contours of minimum B for URAGAN-2M indicate that all deeply trapped particles are lost. This should be taken into consideration when choosing the heating method for this device.

ACKNOWLEDGMENTS

This work was initiated and carried out as part of a US-USSR exchange in fusion research. The authors are grateful to J. F. Lyon, J. H. Harris, O. S. Pavlichenko, and K. N. Stepanov for their support. D. L. Grekov and A. A. Shishkin express their gratitude to ORNL for hospitality and making possible the completion of this work. We also thank Dr. S. P. Hirshman for making available to us the VMEC code used in the present calculations.

REFERENCES

[1] Lyon, J. F., Carreras, B. A., Chipley, K. K., Cole, M. J., Harris, J. H., Jernigan, T. C., Johnson, R. L., Lynch, V. E., Nelson, B. E., Rome, J. A., Sheffield, J., Thompson, P. B., Fusion Technol. **10** (1986) 179.

[2] Bykov, V. E., Georgievsky, A. V., Demchenko, V. V., Kuznetsov, Yu. K., Litvinenko, Yu. A., Longinov, A. V., Pavlichenko, O. S., Rudakov, V. A., Stepanov, K. N., Tolok, V. T., Fusion Technol. **17** (1990) 140.

[3] Besedin, N. T., Kuznetsov, Yu. K., Pankratov, I. M., "The Influence of Helical Conductor Packing on a Magnetic Configuration of an $\ell = 2$ Torsatron with Longitudinal Field," Vopr. At. Nauki Tekh. (Questions At. Sci. Tech.): Thermonuclear Fusion **3** (1987) 18–20 (in Russian).

[4] Bykov, V. E., Shishkin, A. A., Kisslinger, J., Rau, F., "On Vacuum Field Properties on the URAGAN-2M Torsatron Standard Configuration," IPP-2/301, Max-Planck-Institut für Plasmaphysik (August 1989).

[5] Shaing, K. C., Hokin, S. A., Phys. Fluids **26** (1983) 2136.

[6] Dominguez, N., et al., "MHD Ideal Localized Mode Studies for ATF," in preparation (1991).

[7] Bykov, V. E., Volkov, E. D., Georgievsky, A. V., Khodychikh, A. V., Peletminskaya, V. G., Shishkin, A. A., "Neoclassical Transport Coefficients in Modern Stellarator Traps," Vopr. At. Nauki Tekh. (Questions At. Sci. Tech.): Thermonuclear Fusion 4 (1987) 3–6 (in Russian).

[8] Cary, J., Hanson, J., Phys. Fluids **29** (1986) 2464.

[9] Hirshman, S. P., van Rij, W. I., Merkel, P., Comput. Phys. Comm. 43 (1986) 143.

[10] Lee, D. K., Oak Ridge National Laboratory, private communication.

[11] Carreras, B. A., Hicks, H. R., Holmes, J. A., Lynch, V. E., Neilson, G. H., Nucl. Fusion **24** (1984) 1347.

[12] Mercier, C., Nucl. Fusion **1** (1960) 47.

[13] Bauer, F., Betancourt, O., Garabedian, P., Magnetohydrodynamic Equilibrium and Stability of Stellarators (Springer-Verlag, New York, 1984).

[14] Bykov, V. E., Georgievsky, A. V., Peletminskaya, V. G., Khodyachikh, A. V., Shishkin, A. A., Nucl. Fusion **24** (1984) 1195.

[15] Bykov, V. E., Grekov, D. L., Shishkin, A. A., Garcia, L., Harris, J., Rome, J. A., Nucl. Fusion **28** (1988) 871.

[16] Carreras, B. A., Lynch, V. E., Dominguez, N., Leboeuf, J. N., Lyon, J. F., "Confinement Improvement of Low-Aspect-Ratio Torsatrons," ORNL/TM-11101, Oak Ridge National Laboratory (1989).

[17] Hedrick, C. L., Oak Ridge National Laboratory, private communication.

[18] Shaing, K. C., Carreras, B. A., Dominguez, N., Lynch, V. E., Tolliver, J. S., Phys. Fluids B **1** (1989) 1663.

ORNL/TM-11701
Dist. Category UC-427

INTERNAL DISTRIBUTION

1. Director, Fusion Energy Division
2. C. C. Baker
3. M. J. Saltmarsh
4. L. A. Berry
5. R. A. Dory
6. J. L. Dunlap
7. H. H. Haselton
8. M. S. Lubell
9. T. E. Shannon

11–12. Laboratory Records Department
13. Laboratory Records, ORNL-RC
14–15. Central Research Library
16. Document Reference Section
17. Fusion Energy Division Library
18–19. Engineering Technology/Fusion Energy Division Publications Office
20. ORNL Patent Office
21–25. B. A. Carreras
26–30. N. Dominguez
31–35. V. E. Lynch
36–40. J. S. Tolliver

EXTERNAL DISTRIBUTION

Kharkov Institute of Physics and Technology, Academical St. 1, 310108 Kharkov, Ukraina, U.S.S.R.
41–42. V. E. Bykov
43–44. D. L. Grekov
45–46. A. A. Shishkin

47. Office of the Assistant Manager for Energy Research and Development, U.S. Department of Energy, Oak Ridge Operations Office, P.O. Box E, Oak Ridge, TN 37831
48. J. D. Callen, Department of Nuclear Engineering, University of Wisconsin, Madison, WI 53706-1687
49. R. W. Conn, Department of Chemical, Nuclear, and Thermal Engineering, University of California, Los Angeles, CA 90024
50. N. A. Davies, Acting Director, Office of Fusion Energy, Office of Energy Research, ER-50 Germantown, U.S. Department of Energy, Washington, DC 20545
51. S. O. Dean, Fusion Power Associates, Inc., 2 Professional Drive, Suite 248, Gaithersburg, MD 20879
52. H. K. Forsen, Bechtel Group, Inc., Research Engineering, P.O. Box 3965, San Francisco, CA 94119
53. R. W. Gould, Department of Applied Physics, California Institute of Technology, Pasadena, CA 91125
54. R. A. Gross, Plasma Research Laboratory, Columbia University, New York, NY 10027
55. D. M. Meade, Princeton Plasma Physics Laboratory, P.O. Box 451, Princeton, NJ 08543
56. M. Roberts, International Programs, Office of Fusion Energy, Office of Energy

Research, ER-52 Germantown, U.S. Department of Energy, Washington, DC 20545

57. W. M. Stacey, School of Nuclear Engineering and Health Physics, Georgia Institute of Technology, Atlanta, GA 30332
58. D. Steiner, Nuclear Engineering Department, NES Building, Tibbetts Avenue, Rensselaer Polytechnic Institute, Troy, NY 12181
59. R. Varma, Physical Research Laboratory, Navrangpura, Ahmedabad 380009, India
60. Bibliothek, Max-Planck Institut für Plasmaphysik, Boltzmannstrasse 2, D-8046 Garching, Federal Republic of Germany
61. Bibliothek, Institut für Plasmaphysik, KFA Jülich GmbH, Postfach 1913, D-5170 Jülich, Federal Republic of Germany
62. Bibliothek, KfK Karlsruhe GmbH, Postfach 3640, D-7500 Karlsruhe 1, Federal Republic of Germany
63. Bibliothèque, Centre de Recherches en Physique des Plasmas, Ecole Polytechnique Fédérale de Lausanne, 21 Avenue des Bains, CH-1007 Lausanne, Switzerland
64. J. Tachon, CEN/Cadarache, Departement de Recherches sur la Fusion Contrôlée, F-13108 Saint-Paul-lez-Durance Cedex, France
65. Bibliothèque, CEN/Cadarache, F-13108 Saint-Paul-lez-Durance Cedex, France
66. Library, AEA Fusion, Culham Laboratory, Abingdon, Oxfordshire, OX14 3DB, England
67. Library, JET Joint Undertaking, Abingdon, Oxfordshire OX14 3EA, England
68. Library, FOM-Instituut voor Plasmafysica, Rijnhuizen, Edisonbaan 14, 3439 MN Nieuwegein, The Netherlands
89. Library, National Institute for Fusion Science, Chikusa-ku, Nagoya 464-01, Japan
70. Library, International Centre for Theoretical Physics, P.O. Box 586, I-34100 Trieste, Italy
71. Library, Centro Richerche Energia Frascati, C.P. 65, I-00044 Frascati (Roma), Italy
72. Library, Plasma Physics Laboratory, Kyoto University, Gokasho, Uji, Kyoto 611, Japan
73. Plasma Research Laboratory, Australian National University, P.O. Box 4, Canberra, A.C.T. 2601, Australia
74. Library, Japan Atomic Energy Research Institute, Naka Fusion Research Establishment, 801-1 Mukoyama, Naka-machi, Naka-gun, Ibaraki-ken, Japan
75. G. A. Eliseev, I. V. Kurchatov Institute of Atomic Energy, P.O. Box 3402, 123182 Moscow, U.S.S.R.
76. V. A. Glukhikh, Scientific-Research Institute of Electro-Physical Apparatus, 188631 Leningrad, U.S.S.R.
77. I. Shpigel, Institute of General Physics, U.S.S.R. Academy of Sciences, Ulitsa Vavilova 38, Moscow, U.S.S.R.
78. D. D. Ryutov, Institute of Nuclear Physics, Siberian Branch of the Academy of Sciences of the U.S.S.R., Sovetskaya St. 5, 630090 Novosibirsk, U.S.S.R.
79. O. Pavlichenko, Kharkov Physical-Technical Institute, Academical St. 1, 310108 Kharkov, U.S.S.R.
80. Deputy Director, Southwestern Institute of Physics, P.O. Box 15, Leshan, Sichuan, China (PRC)
81. Director, The Institute of Plasma Physics, P.O. Box 26, Hefei, Anhui, China (PRC)
82. R. A. Blanken, Experimental Plasma Physics Research Branch, Division of Applied Plasma Physics, Office of Energy Research, ER-542, Germantown, U.S. Department of Energy, Washington, DC 20545
83. D. H. Crandall, Experimental Plasma Physics Research Branch, Division of Applied Plasma Physics, Office of Energy Research, ER-542, Germantown, U.S. Department of Energy, Washington, DC 20545
84. D. Markevich, Division of Confinement Systems, Office of Energy Research, ER-55, Germantown, U.S. Department of Energy, Washington, DC 20545
85. R. H. McKnight, Experimental Plasma Physics Research Branch, Division of Applied Plasma Physics, Office of Energy Research, ER-542, Germantown, U.S. Department of Energy, Washington, DC 20545

86. E. Oktay, Division of Confinement Systems, Office of Energy Research, ER-55, Germantown, U.S. Department of Energy, Washington, DC 20545
87. W. L. Sadowski, Fusion Theory and Computer Services Branch, Division of Applied Plasma Physics, Office of Energy Research, ER-541, Germantown, U.S. Department of Energy, Washington, DC 20545
88. J. W. Willis, Division of Confinement Systems, Office of Energy Research, ER-55, Germantown, U.S. Department of Energy, Washington, DC 205
89. A. Perez Navarro, Division de Fusion, CIEMAT, Avenida Complutense 22, E-28040 Madrid, Spain
90. J. L. Johnson, Plasma Physics Laboratory, Princeton University, P.O. Box 451, Princeton, NJ 08543
91. L. M. Kovrizhnykh, Institute of General Physics, U.S.S.R. Academy of Sciences, Ulitsa Vavilova 38, 117924 Moscow, U.S.S.R.
92. O. Motojima, National Institute for Fusion Science, Chikusa-ku, Nagoya 464-01, Japan
93. S. Okamura, Institute of Plasma Physics, Nagoya University, Chikusa-ku, Nagoya 464, Japan
94. V. D. Shafranov, I. V. Kurchatov Institute of Atomic Energy, P.O. Box 3402, 123182 Moscow, U.S.S.R.
95. J. L. Shohet, Torsatron/Stellarator Laboratory, University of Wisconsin, Madison, WI 53706
96. H. Wobig, Max-Planck Institut für Plasmaphysik, D-8046 Garching, Federal Republic of Germany
97. F. W. Perkins, Princeton Plasma Physics Laboratory, P.O. Box 451, Princeton, NJ 08543
98. T. Obiki, Plasma Physics Laboratory, Kyoto University, Gokasho, Uji, Kyoto, Japan
99. A. Iiyoshi, National Institute for Fusion Studies, Chikusa-ku, Nagoya 464-01, Japan
100. R. E. Mickens, Atlanta University, Department of Physics, Atlanta, GA 30314
101. M. N. Rosenbluth, University of San Diego, La Jolla, CA 92037
102. D. Schnack, SAIC, 10260 Campus Point Drive, San Diego, CA 92121
103. Duk-In Choi, Department of Physics, Korea Advanced Institute of Science and Technology, P.O. Box 150, Chong Ryang-Ri, Seoul, Korea
104. Library of Physics Department, University of Ioannina, Ioannina, Greece
105. C. De Palo, Library, Associazione EURATOM-ENEA sulla Fusione, CP 65, I-00044 Frascati (Roma), Italy
106. Theory Department Read File, c/o D. W. Ross, Institute for Fusion Studies, University of Texas, Austin, TX 78712
107. Theory Department Read File, c/o R. Parker, Director, Plasma Fusion Center, NW 16-202, Massachusetts Institute of Technology, Cambridge, MA 02139
108. Theory Department Read File, c/o R. White, Princeton Plasma Physics Laboratory, P.O. Box 451, Princeton, NJ 08543
109. Theory Department Read File, c/o L. Kovrizhnykh, Lebedev Institute of Physics, Academy of Sciences, 53 Leninsky Prospect, 117924 Moscow, U.S.S.R.
110. Theory Department Read File, c/o B. B. Kadomtsev, I. V. Kurchatov Institute of Atomic Energy, P.O. Box 3402, 123182 Moscow, U.S.S.R.
111. Theory Department Read File, c/o T. Kamimura, National Institute for Fusion Studies, Nagoya 464, Japan
112. Theory Department Read File, c/o C. Mercier, Departemente de Recherches sur la Fusion Controlee, B.P. No. 6, F-92260 Fontenay-aux-Roses (Seine), France
113. Theory Department Read File, c/o T. E. Stringer, JET Joint Undertaking, Abingdon, Oxfordshire OX14 3EA, United Kingdom
114. Theory Department Read File, c/o R. Briscoe, AEA Fusion, Culham Laboratory, Abingdon, Oxfordshire OX14 3DB, United Kingdom
115. Theory Department Read File, c/o D. Biskamp, Max-Planck-Institut fur Plasmaphysik, Boltzmannstrasse 2, D-8046 Garching, Federal Republic of Germany
116. Theory Department Read File, c/o T. Takeda, Japan Atomic Energy Research Institute, Tokai Fusion Research Establishment, Tokai-mura, Naka-gun, Ibaraki-ken, Japan

117. Theory Department Read File, c/o J. Greene, General Atomics, P.O. Box 85608, San Diego, CA 92138-5608
118. Theory Department Read File, c/o R. Cohen, Lawrence Livermore National Laboratory, P.O. Box 5511, Livermore, CA 94550
119. Theory Department Read File, c/o R. Gerwin, CTR Division, Los Alamos National Laboratory, P.O. Box 1663, Los Alamos, NM 87545

120–167. Given distribution as shown in OSTI-4500, Magnetic Fusion Energy (Category Distribution UC-427, Theoretical Plasma Physics)